Final Technical Report
COVER PAGE

Project Title: Assimilation of Wave Imaging Radar Observations for Real-time Wave-by-Wave Forecasting

Award Number: DE-EE0006789

Project Period: October 1, 2014 – December 31, 2016

Principle Investigator: Merrick Haller, Professor
School of Civil & Construction Engineering
Oregon State University
merrick.haller@oregonstate.edu, 541-737-9141

Recipient: Oregon State University
Office of Sponsored Programs
B308 Kerr Administration Bldg
Corvallis, OR 97331

Other Project Team Members:

Oregon State University — Alexandra Simpson, Graduate Research Assistant
Randy Pittman, Faculty Research Assistant, OSU

SRI International — Dr. David Walker, david.walker@sri.com, 734-926-4416

University of Southern California — Dr. Patrick Lynett, plynett@usc.edu

Date of Report: August 29, 2017

Report Submitted by: Merrick Haller

Acknowledgment: This report is based upon work supported by the U.S. Department of Energy under Award NoDE-EE0006789.

Disclaimer: Any findings, opinions, and conclusions or recommendations expressed in this report are those of the author(s) and do not necessarily reflect the views of the Department of Energy.

CONTENTS

TABLES

FIGURES

1. Executive Summary

This project addressed Topic 3: "Wave Measurement Instrumentation for Feed Forward Controls" under the FOA number DE-FOA-0000971. The overall goal of the program was to develop a phase-resolving wave forecasting technique for application to the active control of Wave Energy Conversion (WEC) devices. We have developed an approach that couples a wave imaging marine radar with a phase-resolving linear wave model for real-time wave field reconstruction and forward propagation of the wave field in space and time. The scope of the project was to develop and assess the performance of this novel forecasting system. Specific project goals were as follows:

- Develop and verify a fast, GPU-based (Graphical Processing Unit) wave propagation model suitable for phase-resolved computation of nearshore wave transformation over variable bathymetry.
- Compare the accuracy and speed of performance of the wave model against a deep water model in their ability to predict wave field transformation in the intermediate water depths (50 to 70 m) typical of planned WEC sites.
- Develop and implement a variational assimilation algorithm that can ingest wave imaging radar observations and estimate the time-varying wave conditions offshore of the domain of interest such that the observed wave field is best reconstructed throughout the domain and then use this to produce model forecasts for a given WEC location.
- Collect wave-resolving marine radar data, along with relevant in situ wave data, at a suitable wave energy test site, apply the algorithm to the field data, assess performance, and identify any necessary improvements.
- Develop a production cost estimate that addresses the affordability of the wave forecasting technology and include in the Final Report.

The developed forecasting algorithm ("Wavecast") was evaluated for both speed and accuracy against a substantial synthetic dataset. Early in the project, performance tests definitively demonstrated that the system was capable of forecasting in real-time, as the GPU-based wave model backbone was very computationally efficient. The data assimilation algorithm was developed on a polar grid domain in order to match the sampling characteristics of the observation system (wave imaging marine radar). For verification purposes, a substantial set of synthetic wave data (i.e. forward runs of the wave model) were generated to be used as ground truth for comparison to the reconstructions and forecasts produced by Wavecast. For these synthetic cases, Wavecast demonstrated very good accuracy, for example, typical forecast correlation coefficients were between 0.84-0.95 when compared to the input data. Dependencies on shadowing, observational noise, and forecast horizon were also identified.

During the second year of the project, a short field deployment was conducted in order to assess forecast accuracy under field conditions. For this, a radar was installed on a fishing vessel and observations were collected at the South Energy Test Site (SETS) off the coast of Newport, OR. At the SETS site, simultaneous in situ wave observations were also available owing to an ongoing

field project funded separately. Unfortunately, the position and heading information that was available for the fishing vessel were not of sufficient accuracy in order to validate the forecast in a phase-resolving sense. Instead, a spectral comparison was made between the Wavecast forecast and the data from the in situ wave buoy. Although the wave and wind conditions during the field test were complex, the comparison showed a promising reconstruction of the wave spectral shape, where both peaks in the bimodal spectrum were represented. However, the total reconstructed spectral energy (across all directions and frequencies) was limited to 44% of the observed spectrum.

Overall, wave-by-wave forecasting using a data assimilation approach based on wave imaging radar observations and a physics-based wave model shows promise for short-term phase-resolved predictions. Two recommendations for future work are as follows: first, we would recommend additional focused field campaigns for algorithm validation. The field campaign should be long enough to capture a range of wave conditions relevant to the target application and WEC site. In addition, it will be crucial to make sure the vessel of choice has high accuracy position and heading instrumentation (this instrumentation is commercially available but not standard on commercial fishing vessels). The second recommendation is to expand the model physics in the wave model backbone to include some nonlinear effects. Specifically, the third-order correction to the wave speed due to amplitude dispersion would be the next step in order to more accurately represent the phase speeds of large amplitude waves.

2. Introduction

A key task in Wave Energy Converter (WEC) development is to optimize device performance for commercial viability. A promising optimization tool is an active control system, which tunes WEC performance to characteristics of the incoming wave field. This enables maximization of energy capture, and potentially protection of the device from extreme waves as well. Accurate and optimal control of WEC devices depends on real-time, phase-resolved wave forecasts on time horizons of the order of several to tens of wave periods. While considerable research has been conducted on WEC control schemes, the mechanism for providing accurate wave forecasts over these time horizons remains an open question.

This project addressed the challenge of wave-by-wave forecasting for WEC controls applications. The targeted time horizon for forecasting was 3–5 min over spatial domains approximately 3–5 km on a side. The technology combines three components: 1) a GPU-based wave model backbone, 2) a wave imaging marine radar observing system, and 3) a data assimilation algorithm. Under this project, the components were combined into a novel wave forecasting system called “Wavecast”. The components are described in more detail below.

Wave model backbone: The wave model backbone contains the governing physics for wave propagation in space and time. The wave model was chosen by considering the application to WEC devices and the expected wave environment at offshore wave energy test sites. For this project, we utilized a wave model based on the Mild Slope Equations (MSEs) as they are fast and efficient to use for waves in intermediate water depths, where refraction, shoaling, and dispersion are all important. The model utilizes a polar grid domain in order to match the sampling scheme of marine radars. The project used the MSEs in their linear form. However, by adding nonlinear correction

terms, the MSEs are capable of accounting for second order stokes nonlinearities. This is a potential future addition to the model.

Wave-imaging marine radar: These systems are commercially available and are standard installations on all non-recreational ocean-going vessels. For this project, radar observations were collected using a Si-Tex (*Radarpc25.9*) X-band imaging radar. The radar was mounted onboard a charter fishing vessel called the *Umatilla II*. Observations were collected offshore of Newport, OR at the South Energy Test Site (SETS) operated by the Northwest National Marine Renewable Energy Center. The radar image data are used to estimate the "radial slope" (the slope of the wave surface in the azimuthal look-direction of the radar beam) using a recently derived relationship to radar backscatter intensity (Lyzenga & Walker, 2015).

Data assimilation algorithm [*Wavecast*]: The complete forecasting algorithm, Wavecast, is a set of modules built to run on GPU (graphical processing unit) hardware. The algorithm uses radial slope data as input and produces a reconstruction and prediction of water surface elevation at all grid points within the model domain. Wavecast applies a variational inverse-modeling approach that utilizes the adjoint of the underlying wave model backbone in order to produce the wave hindcast/forecast. Like all phase-resolving wave models, the necessary input to the wave model backbone is the time varying, offshore boundary condition (typically, surface elevation time series along the offshore boundary). Hence, the data assimilation algorithm estimates the time-varying offshore boundary condition that will yield a wave field simulation that is a best fit to a set of radar observations (e.g. 5-10 minute sequences of radar images). This can then be used to propagate the waves forward in space and time beyond the footprint of the input data to produce the forecast.

Starting from an initial guess for the wave field (typically, simply a flat sea surface), a solution of the wave model adjoint is used to compute the gradient of the error in the initial solution with respect to the offshore boundary condition. This gradient is then used to compute an update to the time-varying offshore boundary condition that reduces the error between the wave field reconstruction and the observations. This process is iterated until the error is reduced to an acceptable level and the best reconstruction of the observed waves in the domain. In the present implementation, the radar images are parsed into discrete time intervals over a partial annular region near the offshore boundary of the domain of interest. Wavecast then assimilates the observations from each interval to produce the reconstructions and forecasts across the entire domain, each of these are then appended in order to produce a 'seamless'nowcast/forecast of the waves in the domain. This output includes wave propagation into the near-field target area (e.g. a WEC array) providing a short-term (several minutes) prediction of the waves expected at the target area in the interior of the domain. The expectation is that the wave forecasts can be utilized to estimate excitation forces, oscillation velocities, or air pressures inside a device in real-time for WEC feed-forward control.

3. Background

There are two main approaches to forecasting that have been proposed in the existing literature. One method aims to make wave predictions at the WEC location using a purely mathematical/statistical model. The idea is to record surface elevation or excitation forces at the target location (e.g. at the WEC), and predict into the future based on the past record. This scheme is illustrated in Figure 1 (a). Proposed approaches using this scheme include decomposition of the signal into individual frequency components (Halliday et al., 2011), or autoregressive methods

such as linear auto regression and neural networks (Fusco & Ringwood, 2010a, 2010b; Schoen et al., 2011). Forecasting based on these purely computational approaches (i.e. not physics-based) has been shown to work for one to two wave periods, but beyond that the accuracy of the forecast breaks down. A competing idea is illustrated in Figure 1 (b), which is often referred to as Deterministic Sea Wave Prediction (DSWP). This idea is to observe the sea surface at a distance from the target forecast point, then use a wave model to reconstruct and propagate the wave field forward in space and time. If the modeled waves can be propagated to the WEC faster than the transit time of the actual waves, a forecast can be made.

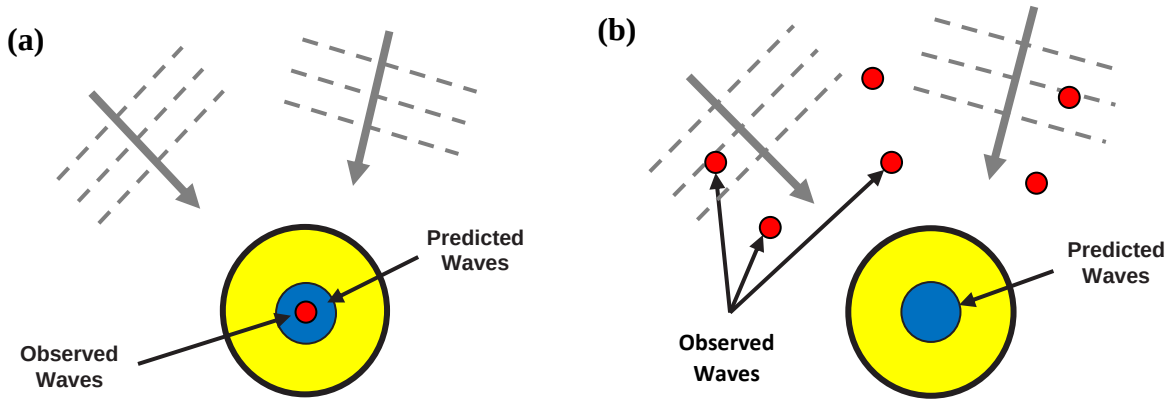

Figure 1. Two main approaches to wave-by-wave forecasting (figure based on Fusco & Ringwood, 2010a): (a) forecast in time using wave record at point location and (b) forecast in space and time using observations at a distance.

Our work used the latter approach. DSWP is a relatively new area of research with limited literature, the majority of which is designed for vessel motion forecasting applications. While some work has been undertaken on the forecasting of nonlinear waves (e.g. Wu, 2004; Blondel et al., 2008; Zhang et al., 1999), computational time requirements have not yet allowed for the utilization of such approaches in real-time. For practical applications, previous work has mainly used linear wave theory without refraction/diffraction effects (Belmont et al., 2003; Belmont et al., 2006; Belmont et al., 2014;). Since many applications are for marine operations, DSWP methods are often focused on the prediction of quiescent intervals (Belmont, et al., 2006; Belmont et al., 2014). Knowledge of these intervals may be sufficient for nautical applications such as cargo transfer and helicopter landing; however, for WEC control applications a continuous forecast is desired (with perhaps additional emphasis on extreme events).

In DSWP, observations of the sea surface at a distance from the target are the needed input to the wave model. Such observations are collected either from a set of wave buoys that record water surface elevation time series, or via a remote sensor, which collects signal from thousands of discrete observation points throughout the spatial domain, but remote sensing data are generally noisier and less direct measurements of water surface elevation. Using a small number of direct observation points with DSWP has been shown to present challenges in multi-directional seas (Janssen et al., 2001; Belmont et al., 2014). Additionally, the deployment of large numbers of wave

buoys can be costly, and real-time transmission of the wave data to the forecast system presents an added operational challenge.

Remote sensing offers the benefit of a much larger data stream; however, a long-dwell platform is necessary (i.e. satellites won't work). Lidar has been proposed as a remote sensor, but is most effective for sea surface observations when operated at small incidence angles (i.e. high altitudes), thus limiting the observation range (Belmont et al., 2008). A plausible option is the wave imaging marine radar, which is well known for its ability to image ocean waves via the tilt-induced modulations of radar backscatter intensity. Radar is also an attractive remote sensing tool because of its existing widespread nautical use, its reasonable cost, and its ability to image waves at distances of 1-3 km.

The project team involved Drs. Merrick Haller, David Walker, and Patrick Lynett. Dr. Merrick Haller (Oregon State University) served as the overall team leader and has 17 years of experience in the collection and analysis of remote sensing observations in order to study wave transformation processes. His group maintains two real-time, shore-based marine radar observing stations in Oregon and he is one of the founding Principle Investigators of the DOE-funded Northwest National Marine Renewable Energy Center. The other members of the OSU team include Randy Pittman (Faculty Research Assistant) who is the radar engineer and Alexandra Simpson (Graduate Research Assistant) who performed substantial data analysis, synthesis and reporting.

Team member Dr. David Walker (SRI International, Ann Arbor, MI) has twenty-five years of experience in conceiving and executing research and development programs in ocean remote sensing, wave and circulation modeling, assimilation of remote sensing data, and algorithm development. In the past five years, he has served as Primary Investigator on over $7 million of government contracts with ONR for remote sensing and data assimilation work. He has previously developed algorithms for estimation of deep water waves from shipboard marine radars for the purpose of environmental situational awareness.

Team Member Dr. Patrick Lynett (University of Southern California) has been working in the field of wave modeling for 15 years. He is the developer of the COULWAVE Boussinesq wave model used for coastal and ocean wave propagation.

4. Results and Discussion

4.1. GPU-based Wave Model

The structure of the Wavecast algorithm is summarized in Figure 2. Choosing the wave model backbone for Wavecast was done with consideration of the application to the existing WEC sites offshore of Newport, OR. Existing phase-resolving wave models that are applicable to non-deepwater conditions are limited to those based on either the Boussinesq equations or the Mild-Slope Equations (MSEs). Other options, such as nonlinear spectral models, potential flow models, and Navier-Stokes models are not yet possible to solve in faster than real time, as needed. In order to choose between the Boussinesq and MSEs, the wave climatology at the SETS offshore of Newport, OR was reviewed. Figure 3 illustrates the conditions in the context of wave model physics. The horizontal axis is a non-dimensional parameter representing relative water depth, and the vertical axis is nondimensional wave height. The points on the plot are derived from historic

data from the field site and represent the potential combinations of wave height, wave period, and water depth. The range of parameters was wave height, 1-8 m, wave period, 6-16 seconds, and water depth, 30-80 meters. The majority of the wave conditions fall in the wave model regions of linear and second-order stokes waves. Hence, it was determined to proceed with a linear wave model based on the MSEs.

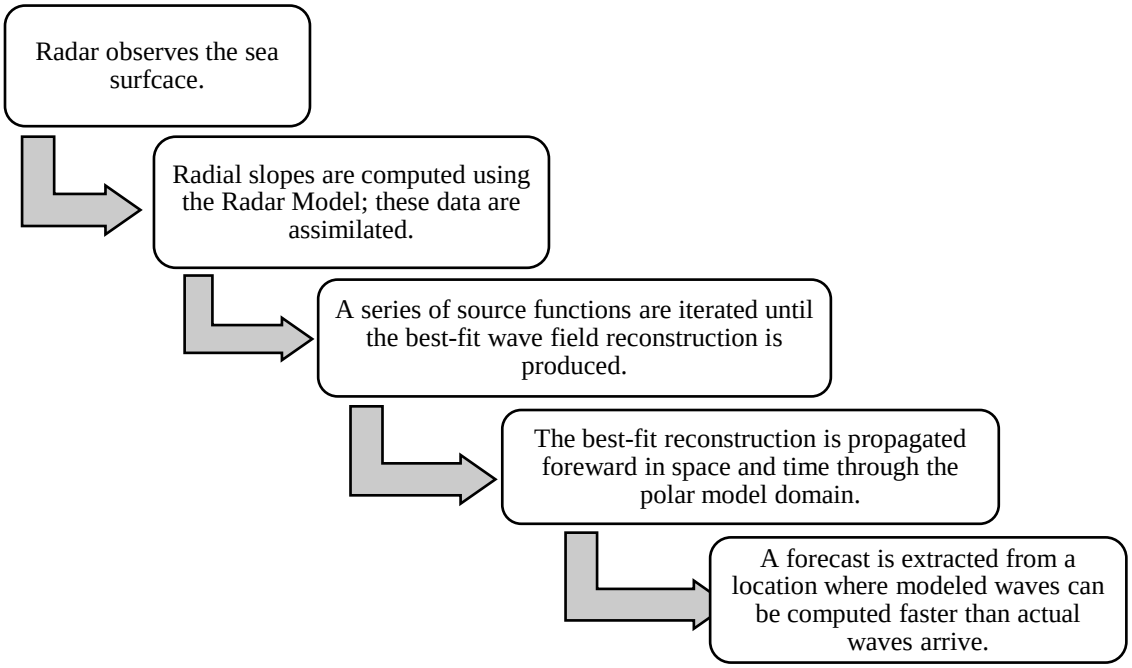

Figure 2. Structure of the Wavecast algorithm.

The MSEs are widely used in regions of intermediate water depths where wave breaking is less important but refraction and diffraction are non-negligible. Originally derived by Berkhoff (1972), they can be divided into a set of hyperbolic, time-dependent equations given by:

$$\frac{\partial \eta}{\partial t} + \nabla \cdot \left[\frac{CC_g}{g}\nabla\phi\right] + \frac{\left(\omega^2 - k^2 CC_g\right)}{g}\phi = 0 \tag{1}$$

$$\frac{\partial \phi}{\partial t} + g\eta = 0 \tag{2}$$

The current version of Wavecast is configured using these equations. However, by using nonlinear correction terms, the MSEs can account for second order stokes nonlinearities. Implementing the nonlinear correction terms is potential future work from this project.

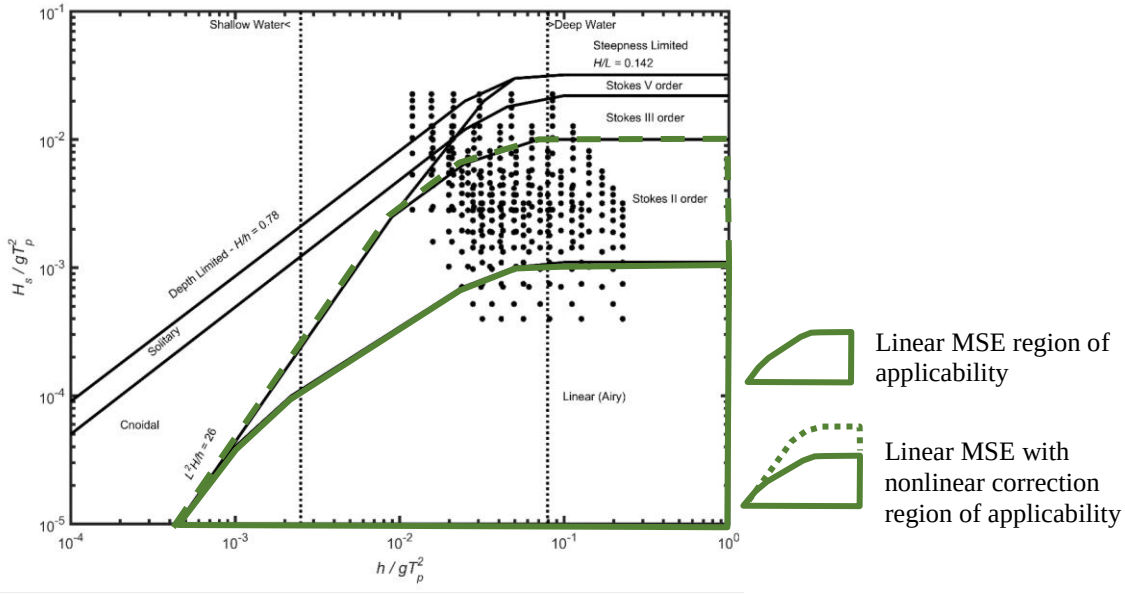

Figure 3. Wave conditions typical of a WEC site, with regions of MSE applicability.

4.2. Radar Post-Processing Algorithm

X-band marine radars are commercially available and standard installations on all non-recreational ocean-going vessels. For this project, radar observations were collected by a Si-tex (Radarpc25.9) X-band imaging radar. The role of the radar in the forecasting system is to collect observations of the sea surface over a 2-3 km radius region surrounding the WEC. The raw data recorded by the radar are values of backscatter intensity, which is a relative measure that is dependent on sea surface roughness at the "Bragg" wavelengths (~3cm) and the relative angle between the water surface and the radar beam, but is not a direct measure of either. A radar imaging model is needed to extract wave information from these images. In this work, we utilized a recently derived radar imaging model that directly links the backscatter intensity, *I*, from a horizontally polarized radar operating at low grazing angles and the radial slope, η_r, of the ocean surface without the need for external calibration as follows:

$$\eta_r(r,\phi) = \frac{h}{r}\left[\frac{I(r,\phi)}{\langle I(r,\phi)\rangle} - 1\right]. \quad (3)$$

Using knowledge of the radar height, *h*, the radial component of the sea surface slope in the radar look-direction, $\eta_{r,}$ can be computed at each range, *r*, and azimuth angle, ϕ. The value $\langle I(r,\phi)\rangle$ is the local mean of intensity at each range and azimuth location. For the full derivation of the radar model, the reader is directed to Lyzenga and Walker (2015). The radial slope is the parameter used for data assimilation in Wavecast.

Wave shadowing is accounted for using knowledge of the radar's baseline noise, where all values falling below this noise level are considered shadowed and masked out of the observation data. The remaining illuminated pixels are considered to have wave information. The radar model is applied to these data, transforming the intensity into radial slope. This pre-processing is performed on the radar data before assimilation into the Wavecast algorithm.

4.3. Forecast Algorithm Development

The data assimilation algorithm applies a variational inverse-modeling approach that utilizes the adjoint of the underlying wave model backbone in order to determine the initial conditions necessary for the wave forecast. Like all phase-resolving wave models, the necessary input to the wave model backbone for prediction in nearshore regions is the time varying off-shore boundary condition. Hence, the objective of the data assimilation algorithm is to estimate the time-varying offshore boundary condition that will yield a wave field simulation that is a best fit to a set of radar observations (e.g. 5-10 minute sequences of radar images).

Starting from an initial guess for the wave field (typically, simply a flat sea surface), a solution of the wave model adjoint is used to compute the gradient of the error in the initial solution with respect to the offshore boundary condition. This gradient is then used to compute an update to the time-varying offshore boundary condition that reduces the error between the wave field reconstruction and the observations. This process is iterated until the error is reduced to an acceptable level and the best reconstruction of the observed waves in the domain. In the present implementation, the radar images are parsed into discrete time intervals over a partial annular region near the offshore boundary of the domain of interest. Wavecast then assimilates the observations from each interval to produce the reconstructions and forecasts across the entire domain, each of these are then appended in order to produce a 'seamless'nowcast/forecast of the waves in the domain.

Solving for the source function is accomplished by including a source *S* in the MSEs, then solving iteratively:

$$\eta_t = -\nabla \cdot (CC_g \nabla\phi) + (\omega^2 - k^2 CC_g)\phi + S \quad (4)$$

$$\phi_t = -\eta, \quad (5)$$

In the MSEs, the first equation solves for the water surface elevation, η, and the second solves for the velocity potential, ϕ, using knowledge of the wave speed C, wave group speed C_g, and wavenumber, k, as a function of position for a fixed angular frequency ω. An important aspect of the MSEs is that they are solved for a single frequency. Thus, the source function is computed for only one frequency at a time. If the spectrum of waves is broad or bimodal, it is necessary to solve the MSEs for each component, thus resulting in several source functions. The resulting single-frequency wave fields will be combined into a complete description of the wave field for final use. Each frequency's source function is determined through an iterative process of minimizing a cost function, which is defined as:

$$J = \iint \frac{1}{2}[\eta_r(x,t) - \eta_r^{obs}(x,t)]^2 M(x,t)\,dx\,dt \quad (6)$$

where η_r is the radial derivative of the model estimated slope, η_r^{obs} is the observed radial slope, and $M(x,t)$ is a shadow mask. The shadow mask is a binary matrix determined from the radar data falling below the noise level, where 1's are illuminated regions of the sea surface, and 0's are shadows in the lee of wave crests. As the model reaches a solution closer to the observations, the cost function is minimized.

We wish to minimize *J* subject to the constraint that the wave field is a solution of the MSEs. The resulting conditions for the minimum leads to a set of adjoint equations:

$$\eta_t = -\nabla \cdot (CC_g \nabla \phi) + (\omega^2 - k^2 CC_g)\phi + S \tag{7}$$

$$\psi_{t'} = -\alpha + M(\eta_r - \eta_r^{obs})_r \tag{8}$$

with

$$\frac{\partial J}{\partial S} = \psi(\mathrm{x}_s, t) \tag{9}$$

as the gradient of the cost function with respect to the source term. The adjoint equations are solved with the error in the present prediction of the radial slope field as input. They are solved backward in time ($t' = -t$) and serve to propagate errors in the prediction back to the time and location of corresponding errors in the source term $S(x_s, t)$. The gradient of *J* with respect to the source term, used to adjust the source term to modify *S* in a way that reduces J is computed from the solution to the adjoint equations as shown.

In each iteration, the wavemaker source *S* is updated using the gradient of the cost function, where b is a constant determined using least-squares estimation:

$$S_{\mathrm{new}} = S - b\psi(\mathrm{x}_s) \tag{10}$$

S is updated with S_{new} for the proceeding iterations. The forward and adjoint equations are solved iteratively until convergence of *J*. This procedure in the algorithm can be summarized in the following steps:

1. Assume a zero initial guess for the source function.
2. Compute the error in the radial slope (source term for the adjoint ψ equation) and execute the adjoint model.
3. Compute the gradient of the cost function with respect to the source function at the wavemaker location from the adjoint solution.
4. Adjust the source function from its initial guess using this gradient.
5. Execute the forward model for a new MSE solution; the cost function will be reduced from step 2.
6. Repeat steps 2-5 until the cost function converges.

These steps are carried out once for every specified frequency in the model configuration. Thus, there will exist a source function for each specified frequency, which may be used independently to propagate waves through the domain. The wave fields from each source function are summed to produce the final wave field.

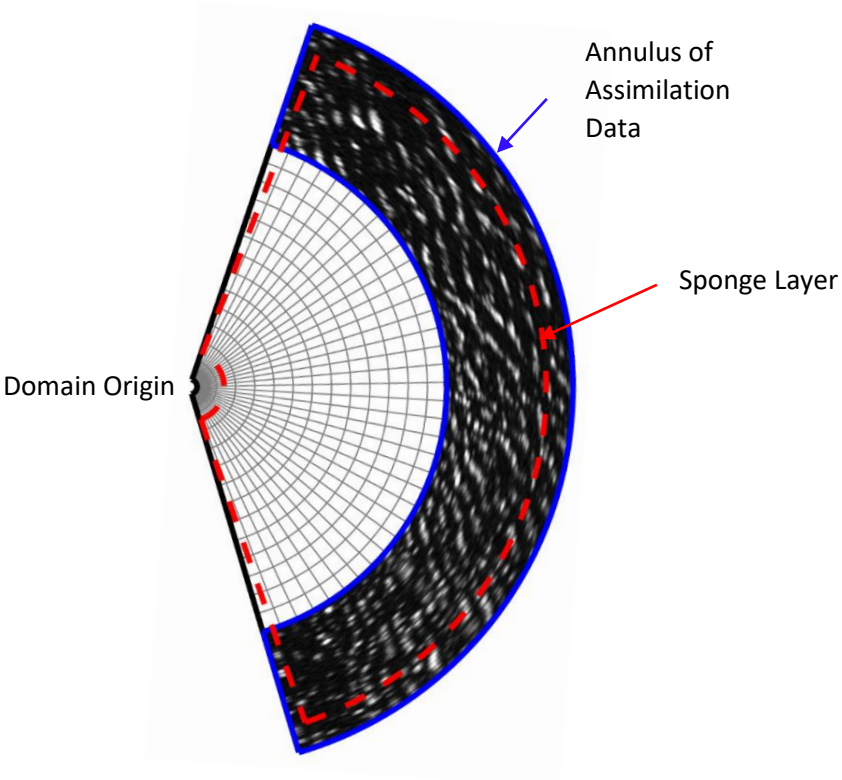

Figure 4. Schematic of Wavecast polar domain. The annulus of data used for assimilation is shown in blue. The sponge layer is outlined in dashed red. The grid lines of the computation domain are shown as grey lines at 1:50 and 1:7 scales for range and azimuth, respectively.

The Wavecast model domain is shown in Figure 4 and encompasses the radar data used for assimilation, as well as an extension of the domain where the forecast is produced. This extension is the region where the target forecast is extracted. The full domain is defined in polar coordinates for compatibility with the range-azimuth collection scheme of radar imagery. In Figure 4, the gray range and azimuth gridlines are a coarsened representation of the model resolution. The resolution of the model domain used in this study is 3 meters in range and 0.7 degrees in azimuth. Sponge layers are drawn as red dashed lines inside of the outer bounds of the computation domain, and are used for minimizing reflection off the boundary walls. Each available radar image would fill up the entire computation domain, however the full scans are not used for data assimilation. Rather, only an annulus at the outer ranges of the radar scan is used. A representation of this assimilation annulus is outlined in blue. Only the outer ranges of the radar scan are used for the sake of reducing computation time; it is shown that an annulus encompassing several wavelengths is enough for estimating the source function. The orientation of this annulus with respect to the location of interest for forecasted waves is important. The annulus must be oriented so that it contains up-wave information, e.g waves travelling towards the location of interest. Additionally, the annulus must be chosen at an optimal range distance from the location of interest. The distance between the inner edge of the assimilation annulus and the location of interest determines how much buffer time the model has for computation. In other words, the travel time of the actual waves in the region is the maximum allowable time for model computation, such that the forecast will be produced before the actual waves arrive. Increasing this distance will increase the time into the future that the waves can be forecasted. However, the distance at which the annulus can be placed

is limited by data quality from the radar. As range increases in a radar scan, so does wave shadowing (i.e. there is less wave information). The annulus must be placed at an optimal range such that forecast time is maximized but high enough data quality is maintained.

The estimated source function is applied for forward propagation along the outermost range of the domain as indicated in Figure 4. From this outermost range, the waves propagate across the domain towards the origin. The location of interest for the forecast can be anywhere within the computation domain inside of the sponge layers. The closer to the origin this location is chosen, the longer the possible forecast time horizon.

4.4. Synthetic Data Generation and Performance Assessment

A synthetic dataset is used for assessment of Wavecast accuracy. The synthetic dataset is generated using the wave model backbone to generate synthetic multidirectional wave fields based on realistic wave spectra and then analytically transforming the surface elevations into radial slopes for assimilation into Wavecast. Noise and shadowing are also added to the radial slope data for a more realistic representation of radar image data, as explained below. An example simulated wave spectrum is shown in Figure 5.

For this spectrum, the significant wave height is 2.4 meters, with a peak period of 10 seconds, and mean wave direction of 270 degrees. The surface elevation time series for this wave field are generated by using the MSEs to propagate the wave components across the polar grid using a uniform water depth of 65 meters. The frequency and direction components are summed to create a synthesized, multi-frequency, and multidirectional wave field. From the surface elevations, the radial slope is computed for assimilation in Wavecast. This is done by taking the finite differenced derivative of the surface elevation along each range line, where for each range r and azimuth φ, the radial slope η_r is:

$$\eta_r(r_i, \phi_i) = \frac{\eta(r_{i+1}, \phi) - \eta(r_{i-1}, \phi)}{2\,\Delta r} \tag{11}$$

Snapshots of the surface elevation and radial slope in polar coordinates are shown in Figure 6. Shadowing is accomplished through simple geometric consideration. Along each range line, the incidence angle, θ, is the angle between the radar beam drawn to the sea surface, and the normal to the location the radar is mounted. If at any range, r, the incidence angle is less than any prior incidence angle, the sea surface at that r is shadowed. A schematic of this is shown in Figure 7.

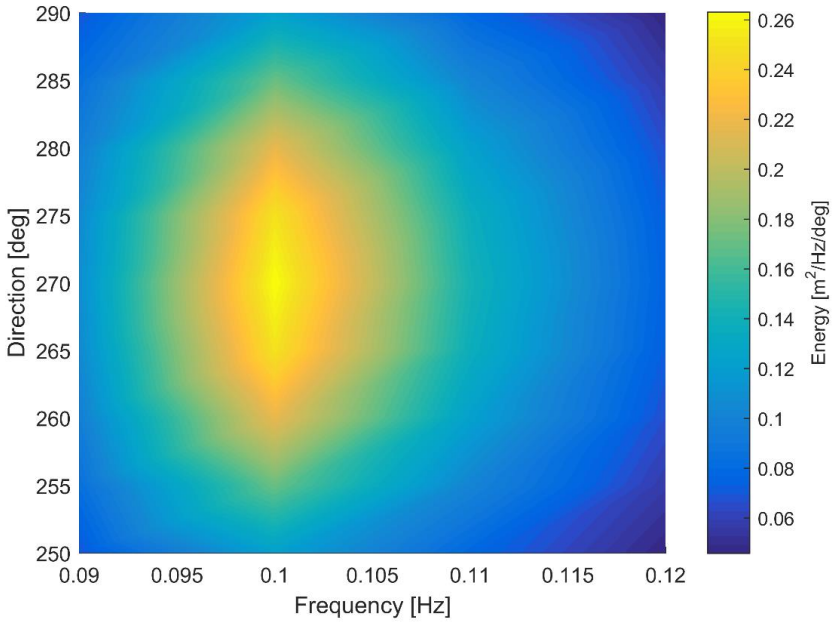

Figure 5. Wave spectrum used for generation of the synthetic dataset.

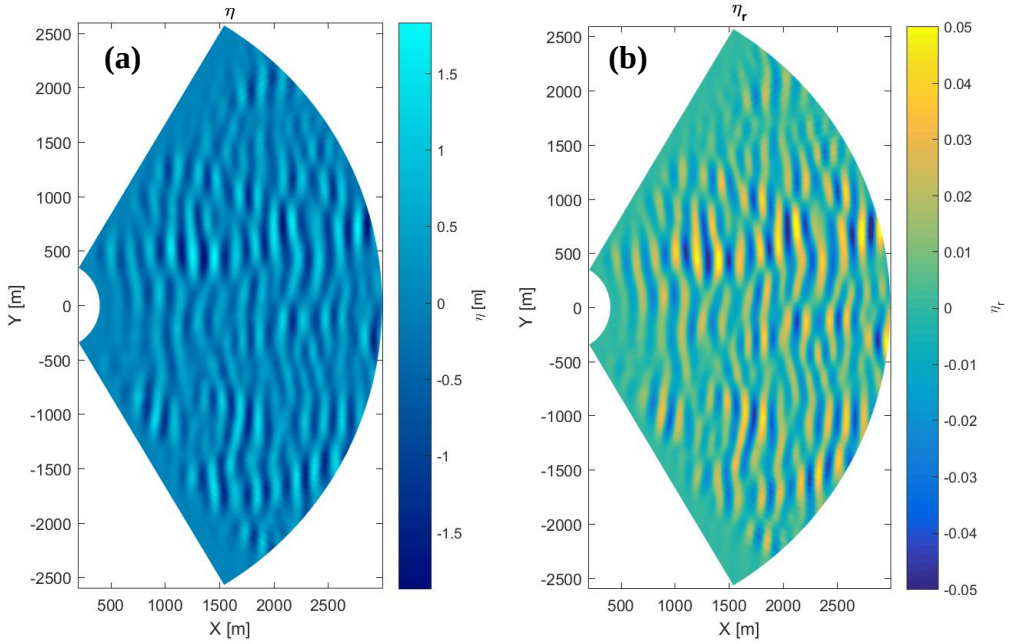

Figure 6. (a) Synthetically generated water surface elevation (b) Radial component of the sea surface slope computed form the surface elevations using a finite difference derivative.

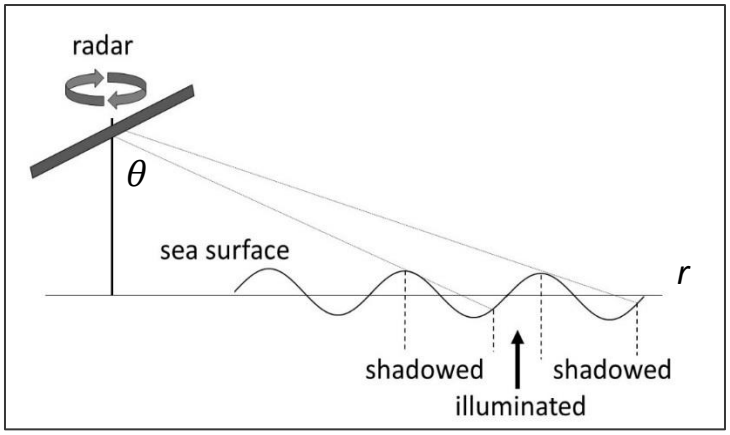

Figure 7. Schematic of wave shadowing.

The thermal noise is simulated by empirically evaluating a radar dataset collected in Newport, Oregon. In the domain of the shore-mounted radar, there is a bluff that blocks the radar signal, leaving a large shadowed region behind it. The intensity of backscatter noise behind the bluff is purely noise. The noise in the raw intensity signal is normally distributed with a mean of 12.2 and a standard deviation of 3.5. A synthetic time series of intensity noise, I_{Nt} can be generated using a normally distributed random number generator; however, the intensity noise must be converted to radial slope noise, η_{rN}, for addition to the radial slope synthetic input. To do this, the radar model (Lyzenga & Walker, 2015) is considered. An empirical constant, ϵ is derived which, when multiplied to the synthetically generated intensity noise, generates random radial slope noise. In equation 13, $I(r, \varphi, t)$ represents the intensity at a location where there is a wave signal (e.g. not behind bluff), I_{N0} is the noise mean computed in the region behind the bluff, and < > is the operator for the local mean.

$$\eta_{rN} = \epsilon I_{Nt}(r, \varphi, t) \tag{12}$$

$$\epsilon = \frac{h}{r}\left[\frac{1}{\langle I(r, \varphi, t) - I_{N0}\rangle}\right] \tag{13}$$

From considering two datasets collected offshore Newport, OR, a best approximation for ϵ is determined to be 0.05. Using geometric shadowing considerations and this derivation of radial slope noise, synthetic datasets are generating using a range of simulated radar heights. With decreasing radar height, shadowing is more prominent in the domain. An example dataset using a 5 meter radar height is shown in Figure 8 (a). The shadowed radial slope with addition of simulated noise is shown in Figure 8 (b). Transects through the shadowed surface elevation and radial slope are shown in Figure 9.

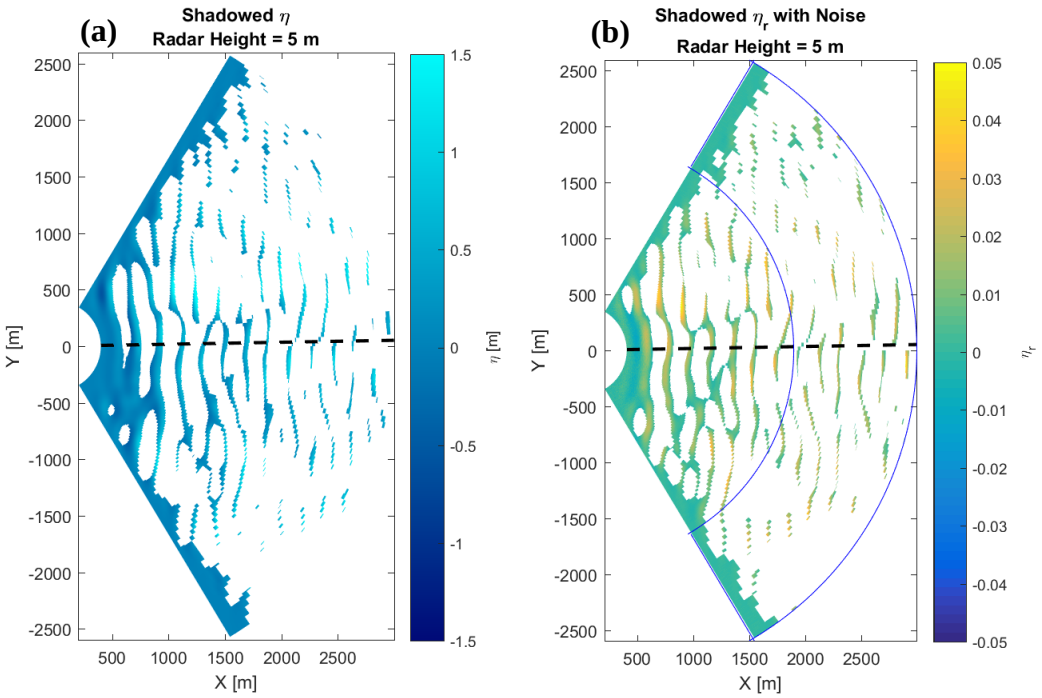

Figure 8. (a) Surface elevations with shadowing applied from a 5 meter high radar. (b) Radial slopes with shadowing applied from a 5 meter high radar, and synthetic thermal noise added. The outlined annulus shows the data assimilated in Wavecast.

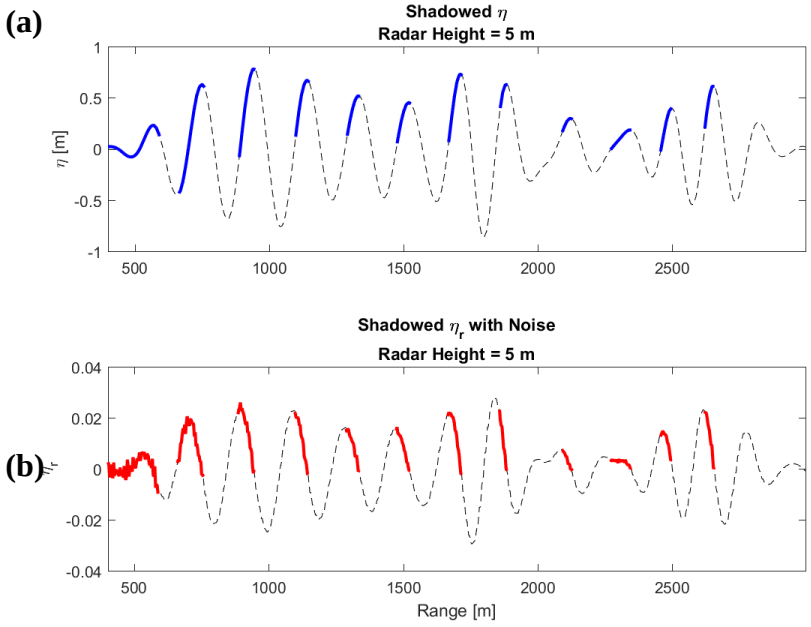

Figure 9. Transects of surface radial slope, both illuminated and shadowed, along the dashed lines shown in Figure 8(a) and (b). (a) Radial slope (dashed line), illuminated portion (blue) along transect in 8(a), (b) radial slope including shadowing and noise and illuminated portion (red) along the dashed line in Figure 8 (b).

The synthetic radial slope data is used for data assimilation in Wavecast. Five trials are presented: four trials of varying radar height with simulated noise, and one trial with no shadowing or noise. Results from these trials are presented in Table 1 and described in more detail here.

The Wavecast output can be assessed for accuracy by comparing time series to the ground truth surface elevation data. Six locations throughout the Wavecast domain are chosen for comparison, as labeled in Figure 10. Locations 1 and 2 are within the assimilation annulus, thus these waves are reconstructed by Wavecast as opposed to predicted. Locations 3 and 4 are outside of the assimilation annulus, thus these time series have been predicted by Wavecast. Locations 1-4 lie along the azimuth of wave propagation. For azimuthal time series comparisons, Locations 5 and 6 are chosen at the same range as Location 1, but varying azimuthally.

At each location, the correlation coefficient between the Wavecast output and ground truth time series is computed. When assimilation data is used without noise or shadowing, the highest correlation is achieved (0.84-0.95 varying by location). With the lowest radar height (2 meters) much of the domain is shadowed, thus the poorest correlation is achieved (0.41-0.9). When shadowing is applied, the outer azimuths at Locations 5 and 6 are the most influenced, as shadowing has a larger influence the more oblique the wave direction. Sample time series correlations are shown in Figure 11 (no noise or shadowing) and Figure 12 (noise and shadowing with 5 m radar height).

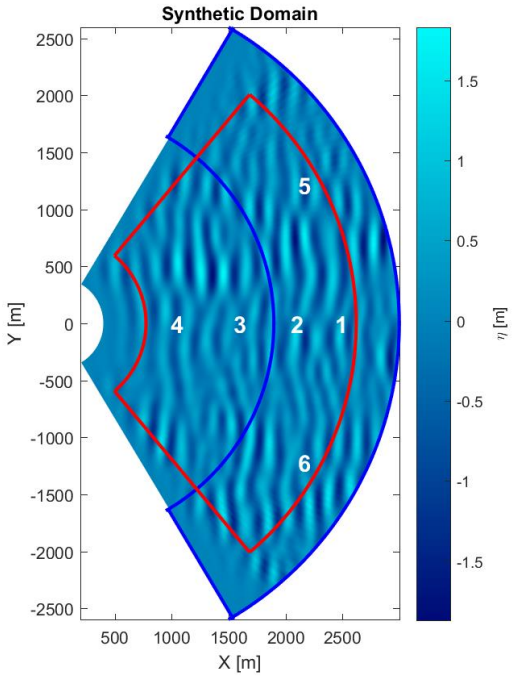

Figure 10. Schematic of synthetic domain used in Wavecast. The annulus used for data assimilation is outlined in blue. The sponge layer is outlined in red. The numbered locations represent points used for time series comparison of Wavecast output to ground truth surface elevations.

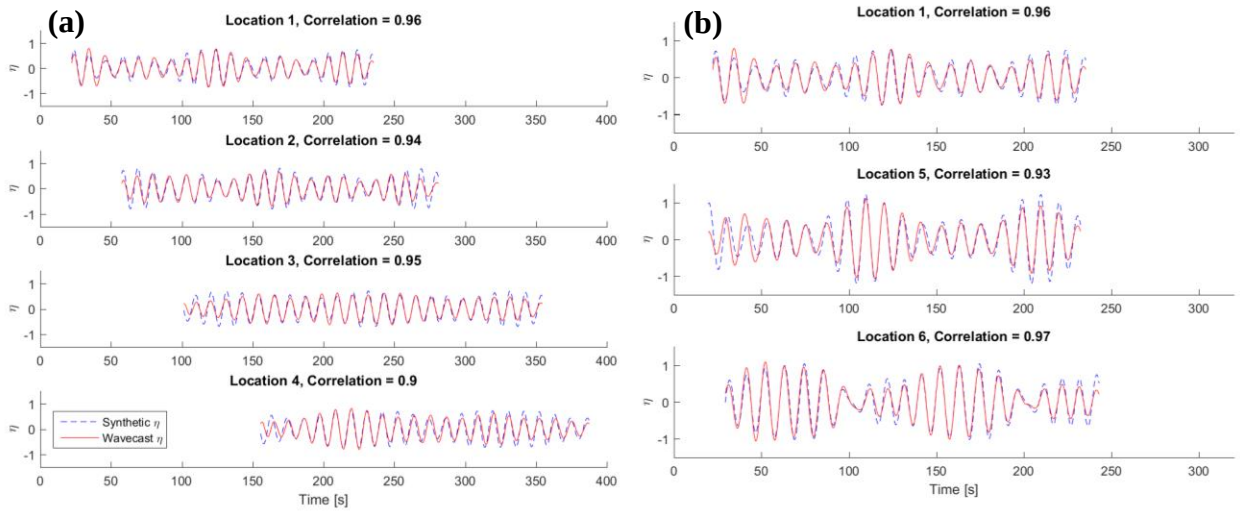

Figure 11. (a) Time series comparison between Wavecast output and synthetic ground truth surface elevations with no noise or shadowing. These time series lie in the direction of wave propagation at various range locations 1-4, as seen in the schematic in Figure 10. (b) Time series comparison between Wavecast output and synthetic ground truth surface elevations with no noise or shadowing. These time series lie along the same range at three azimuthal locations, locations 1, 5 and 6 seen in the schematic in Figure 10.

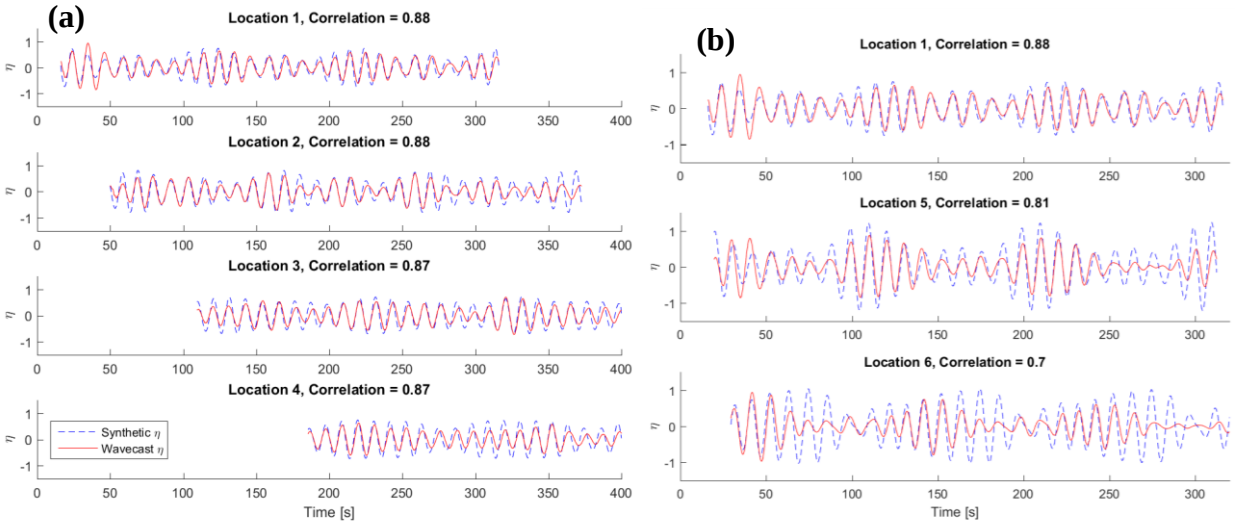

Figure 12. (a) Time series comparison between Wavecast output and synthetic ground truth surface elevations with simulated radar noise and shadowing from a 5m tall radar. These time series lie in the direction of wave propagation at various range locations 1-4, as seen in the schematic in Figure 10. (b) Time series comparison between Wavecast output and synthetic ground truth surface elevations with simulated radar noise and shadowing from a 5m tall radar. These time series lie along the same range at three azimuthal locations, locations 1, 5 and 6 seen in the schematic in Figure 10.

Radar Height (m)	Correlation Coefficient (1 = perfectly correlated)					
	Reconstructed		Predicted		Wide Azimuths	
	1	2	3	4	5	6
2	0.76	0.9	0.78	0.85	0.41	0.48
3	0.79	0.9	0.82	0.86	0.45	0.52
5	0.83	0.88	0.87	0.87	0.59	0.54
10	0.89	0.91	0.9	0.88	0.89	0.74
No noise or shadow	0.93	0.94	0.95	0.9	0.85	0.94

Table 1. Summary of results from synthetic trials with varying simulated radar height.

4.5. Field Data Collection and Performance Assessment

On December 15, 2015, a dataset of radar and in situ surface elevation measurements was collected offshore of Newport, OR. The radar was mounted onboard the *Umatilla II*, a 50 foot charter fishing vessel that can be seen in Figure 13 (a). In situ surface elevation data were being simultaneously recorded by a TRIAXYS Directional Wave Buoy. The TRIAXYS buoy can be seen from onboard the *Umatilla II* in Figure 13 (b). The meteorological conditions on December 15 were complex. A schematic of the data collection is shown in Figure 14.

The frequency spectrum and directional spectrum collected by the TRIAXYS buoy during the field data collection period are shown in Figure 15 (a) and (b), respectively. The spectrum is bimodal; components at both 11 and 20 second periods are present. These are challenging conditions for the Wavecast system because the MSE is solved using a single frequency at a time. Thus, in order to reconstruct both swells, a minimum of two solutions to the MSEs need to be found.

(a)  **(b)** 

Figure 13. (a) Radar mounted on the *Umatilla II*. (b) TRIAXYS buoy as seen from onboard the *Umatilla II*.

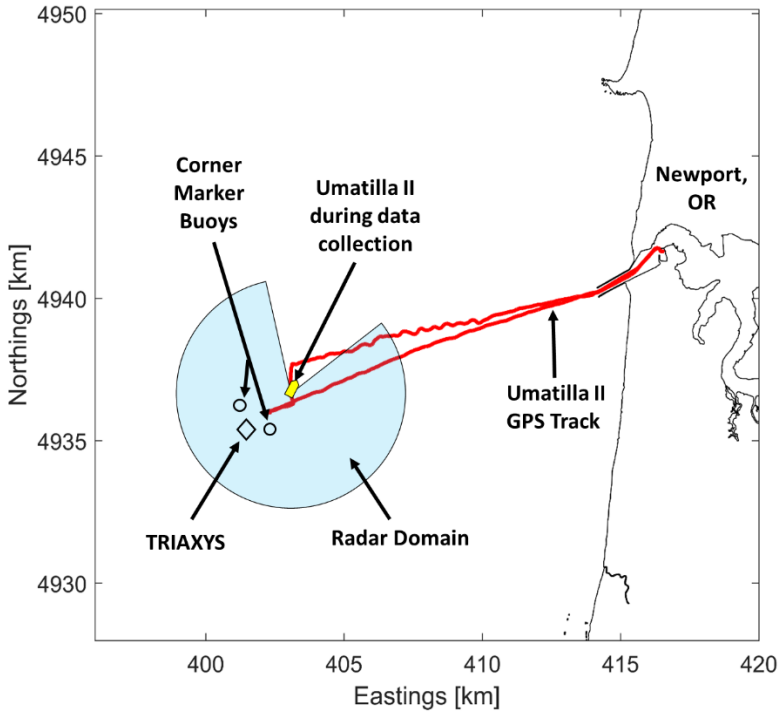

Figure 14. Schematic of field data collection.

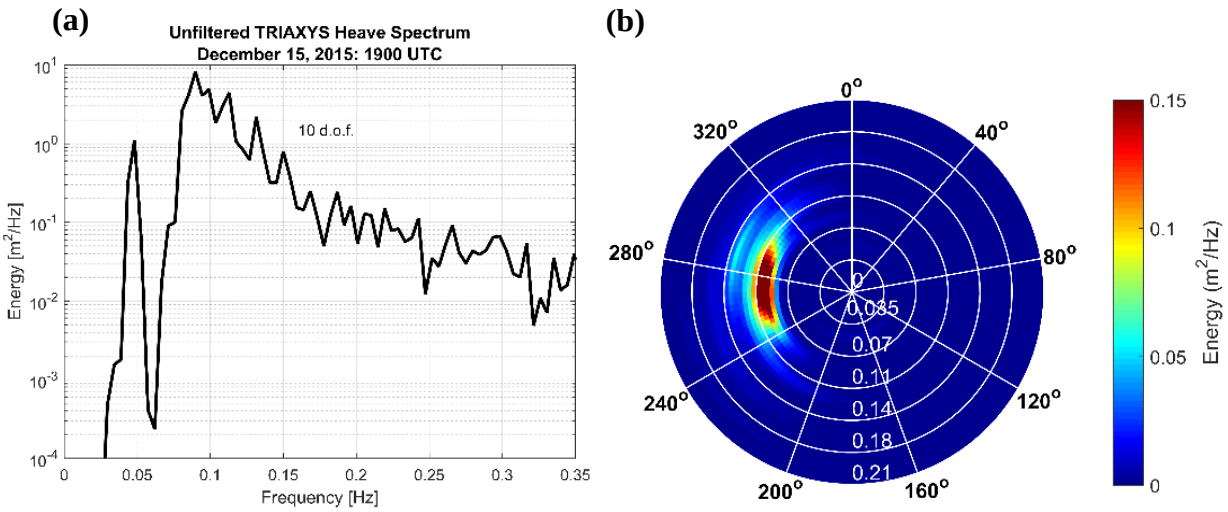

Figure 15. (a) Frequency spectrum recorded by the TRIAXYS during field data collection. (b) Frequency-direction spectrum recorded by the TRIAXYS during field data collection.

An additional challenge during data collection was that the relative wind and wave directions were non-ideal for wave imaging in the radar data. The most optimal radar images are collected when the radar is looking in the same direction as the wind, which yields the maximum amount of surface roughness on the faces of the waves. When the radar is not looking in the same direction as the wind, the radar does not get as strong of a reflection from the surface, and will not see waves as

far out in the domain. Reports from the National Data Buoy Center Station 46050 indicate that throughout the data collection period of the field testing, the wind direction shifted from perpendicular to the radar look direction, to opposite of the radar look direction. It is likely that if the wind were in the same direction as the waves during this collection period, waves would be seen at further ranges. The main effect this has on the field dataset is that the wave signal is weak at the location of the TRIAXYS buoy. In other words, the boat should have been closer to the TRIAXYS to yield a stronger assimilation dataset for forecasting at the TRIAXYS location. In future studies, the wind conditions should be taken into consideration when determining the ranges of radar data used for the assimilation, noting that waves will be imaged at further ranges in the domain when the wind is in the radar look direction.

The electronic compass headings originally recorded for rectification of ship motion using an inexpensive compass were too noisy to be used for effective stabilization and geo-rectification. Thus, a two-part correction scheme was developed that utilizes features within the radar imagery, namely ocean waves and the signatures of two moored buoys. The waves were treated as a stationary image-to-image feature.

Each radar image was cross correlated to the previous image such that the relative rotation that created a maximum wave alignment between the images was found and was assumed to represent the relative ship rotation that occurred between images. The mean of the rotations was removed to account for the fact that the waves are not perfectly stationary, rather propagating through the image. Once the images are reasonably well stabilized using this technique, the signatures of two moored buoys become visible in running averages of the radar images, seen in Figure 16. The buoys were then used in a second cross-referencing scheme, where the location of the buoys in each image is matched to the preceding image. Additionally, the GPS coordinates of the buoys are known with 50 m certainty, so the images can be geo-referenced spatially. The result is a dataset of stabilized and geo-referenced radar data with spatial and temporal overlap to the TRIAXYS buoy data. This radar dataset is used for assimilation, and spectrally validated to the TRIAXYS buoy. Due to lack of adequate precision in the geo-reference scheme, the phase-resolved comparison was not successful.

To prepare the radar intensity data for use in Wavecast, the radial slope of the waves is estimated using the previously described radar model. The radial slopes computed from the stationary radar dataset are used for data assimilation in Wavecast. The domain configuration overlaid on one snapshot of radial slope data is shown in Figure 17. The domain was chosen carefully such that (1) the computation domain contained the location of the TRIAXYS (2) the assimilation domain contained up-wave data and (3) the assimilation domain contained wave data not masked out by shadowing. In this configuration, the TRIAXYS is within the assimilation domain, therefore the modeled waves at this location would not actually be forecasted waves but would be reconstructed waves; however, the purpose of this analysis is to assess overall accuracy potential at this point in time. When assimilating this dataset in Wavecast, two frequencies are chosen for the solution to the MSEs. This is because the seas were bimodal, this there are two major frequency components, which will be propagating at different velocities.

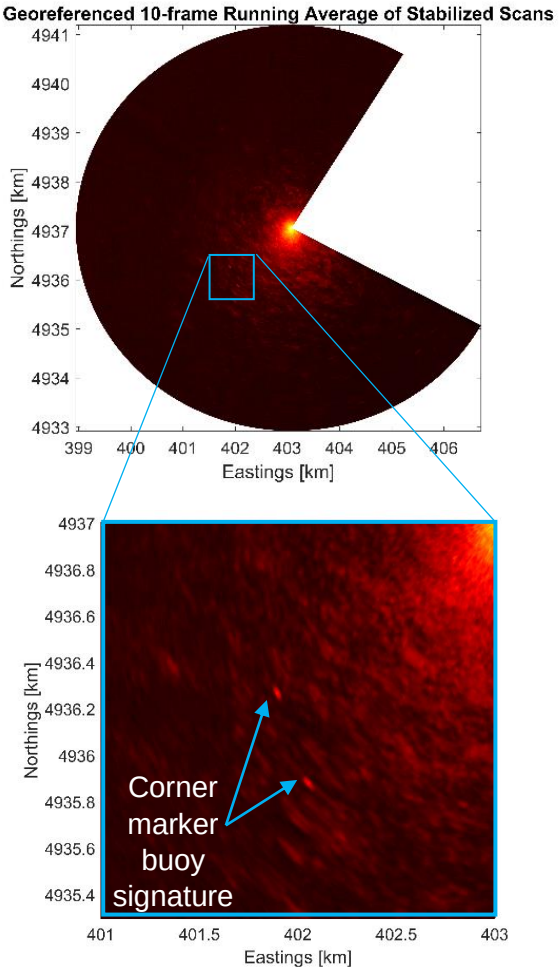

Figure 16. Geo-rectification process for ship-mounted radar data collected on the *Umatilla II.*

As mentioned, a phase-resolved wave comparison was not possible due to the lack of accurate GPS data. However, a spectral comparison between the Wavecast forecasted waves and the in situ buoy observations was still performed. This is presented in Figure 18. In Figure 18 (a) the significant wave height (H_{sig}) is computed throughout the Wavecast model simulation at each location in the domain. From the TRIAXYS buoy data, the anticipated H_{sig} 1.8 meters. The maximum H_{sig} reached in the Wavecast modeled waves is 1.6 meters, with an average H_{sig} throughout the domain of 0.77 meters. A spectral comparison is performed between the TRIAXYS spectrum and the spectrum of modeled waves at the anticipated location of the TRIAXYS, as indicated by the points shown in the Southwest corner of the domain in Figure 18 (a). This spectral comparison is shown in Figure 18 (b). The two peaks in the spectrum are resolved, however only 44% of the spectral energy is reconstructed by Wavecast.

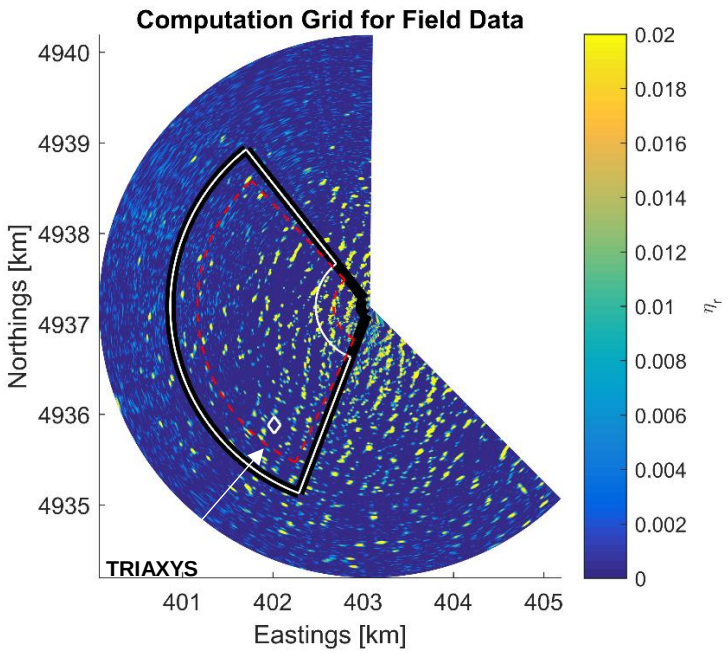

Figure 17. Radial slope estimated from the ship-mounted radar data collected on the *Umatilla II*. The domain used for assimilation and prediction in Wavecast is shown on the image, where the black outline represents the entire Wavecast domain, the white line represents the assimilated data, and the red dashed line shows the sponge layer. The location of the TRIAXYS buoy is indicated.

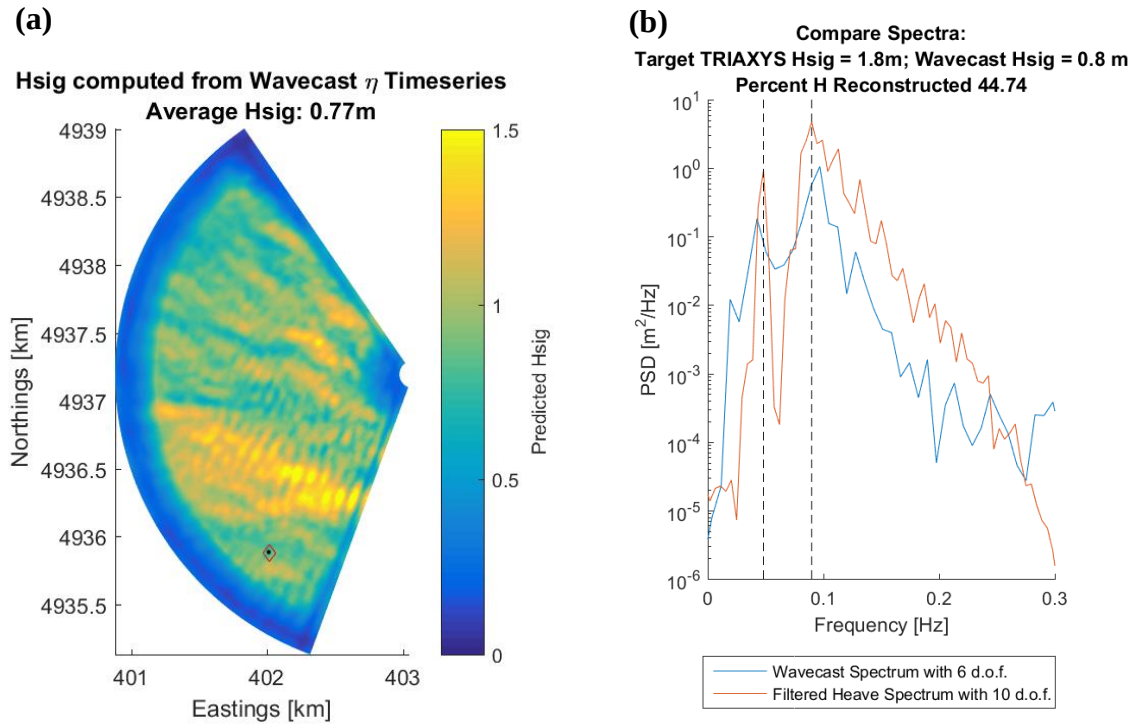

Figure 18. (a) Significant wave height throughout the domain of Wavecast output using assimilation of ship-mounted radar data. (b) Spectral comparison of the TRIAXYS time series to the Wavecast output time series at the estimated location of the TRIAXYS buoy.

Despite adequately reconstructing the shape of the spectrum, a 44% reconstruction of energy is a poor representation of the capabilities of Wavecast. We believe this is due to the quality of the field dataset. The major reasons impacting the quality of the dataset are (1) inability to precisely locate the buoy in the radar image domain (due to rectification uncertainty) and (2) poor orientation of the forecast point (i.e. the TRIAXYS buoy) with respect to the wind and wave direction within the radar images. The main factor influencing (1) is the quality of the GPS heading data used for rectifying the images. There are several factors influencing (2). During collection of the field dataset, the location of the TRIAXYS is on the outskirts of well-defined wave information, as can be seen in Figure 17. There is substantial shadowing in (and up-wave of) the radar imagery at the location of the TRIAXYS. Thus, there is minimal wave information with which Wavecast can reconstruct and predict the waves at the TRIAXYS location. In future field tests, pre-planning the vessel deployment based on wind and wave conditions should lead to a better result. Having shown successful reconstruction of synthetic radial slope with realistic noise and shadowing, there is substantial evidence that Wavecast would perform well given a higher quality field dataset.

4.6. Model Timing Capabilities and Constraints

The analysis of Wavecast performance in this study is focused primarily on performance accuracy. This section defines the domain and computation constraints of making Wavecast operational in real-time. The key requirement of the system is that the data assimilation and forward propagation can be computed in faster than real time. In other words, the modeled waves must be computed at the location of interest before the actual waves arrive.

Wavecast's computation is dependent on a number of tunable parameters. While the data used for assimilation is always radar imagery on a polar domain, the size and duration of assimilation data is tunable. Likewise, while the computation domain is a polar grid nested inside of the assimilation region, the size of this domain determines how long the model takes to perform its computation. A list and description of the tunable parameters is given in Table 2, and a diagram of the parameters on the Wavecast domain is shown in Figure 19.

A time-space diagram of forecast model timing constraints is shown in Figure 20. The y-axis represents one spatial dimension. i.e. range distance. X_{assim} is the size of the assimilation domain in range (meters). The full y-axis represents the entire range of the domain, from the outer edge to the origin. The distance between the assimilation region and the origin is called X_{pred}, and is the distance across which the predicted waves travel to the origin. The x-axis represents time in seconds. The first step in the model is to record the radar observations. The duration over which observations are collected is called T_{obs}. Once the observations are recorded, the data assimilation and calculation phase can begin. The duration of each computation phase is depicted as Δt_{comp}. In this schematic, the computation time was determined using a sample Wavecast trial of synthetic data, with the specified model configuration. During the computation phase, two major steps are achieved (1) the observed data is assimilated for computation of the source function and (2) the source function is propagated from the outer boundary of the domain, through X_{assim} and X_{pred}.

In order to create a forecast, the computation must be performed before the actual waves arrive at the location of interest. Thus, the velocity at which the actual waves travel is considered. The characteristic speed of wave transformation is the group velocity, Cg. This rate is shown as a

diagonal line in Figure 20. The diagonal line is drawn from the inner edge of the assimilation region, because the predicted waves must be computed before the first observed waves arrive at the location of interest. In this schematic, the location of interest is the origin. The time between the completion of the computation and the arrival of the actual waves at the location of interest is the duration in advance that the waves can be forecasted, Δt_{fcst}. In this to-scale schematic, the waves are predicted 75 seconds in advance.

Parameter	Description	Effect on Computation Time
# frequencies	Number of frequencies for which the MSEs are solved.	The Mild Slope Equations are solved once per frequency specified. Thus, the number of frequencies used linearly increases the computation time.
$\mathbf{X_{pred}}$	Range of the computation domain	Increasing the range of the computation domain will linearly increase the computation time, but will also increase the time it takes for the actual waves to propagate across the domain. So far it has been shown that the computation time is faster than the propagation time, thus increasing the range of the computation domain will ultimately increase how far in advance the waves can be forecasted, Δt_{fcst}
$\mathbf{X_{assim}}$	Range of assimilation domain	The size of the assimilation domain has the same impact on forecasting as $X_{pred.}$ An additional influence of X_{assim} is that increasing the assimilation range improves the accuracy of the source function. The assimilation range should be large enough to capture several wavelengths, but should not be extend to a range of the radar image where there is considerable wave shadowing.
$\mathbf{T_{obs}}$	Duration of observations used for assimilation	The computation begins after the assimilation data has been observed. The observations used for assimilation must be long enough to adequately reconstruct the wave field, on the order of tens of wave periods. The minimum observation time should be used while still maintaining forecast accuracy.
Φ	Azimuthal extent of grid	The azimuthal extent of the assimilation region and computation region must be the same. The azimuthal extent should be wide enough to capture the spread of wave directions in the assimilation data. Increasing azimuthal extent will increase computation time.
Sponge layer	Absorption of waves along outer boundaries of domain to prevent reflection.	The sponge layer is a region that absorbs waves along the outermost range of the assimilation region, the outermost azimuths, and the innermost range of the computation domain. It should be at least 1-2 wavelengths. The sponge layer does not have a direct influence on computation time, however the larger it is made the smaller the computation domain.

Table 2. Tunable parameters in Wavecast with a discussion of influence on forecast accuracy and timing.

The forecast available after the computation phase is shown for each model run below the domain origin in Figure 20. The first forecast begins with still water until the arrival of the first waves. Forecasted waves begin at the origin once the first observed waves at the inner edge of the assimilation domain arrive. The duration of the forecast is dictated by the region and duration of the assimilation data. The dashed diagonal line represents the last observed wave at the outer range of the assimilation domain. Since this is the last observed wave, it will be the last wave able to be forecasted. Thus, the duration of the first forecast lasts until the first diagonal dashed line crosses the domain origin.

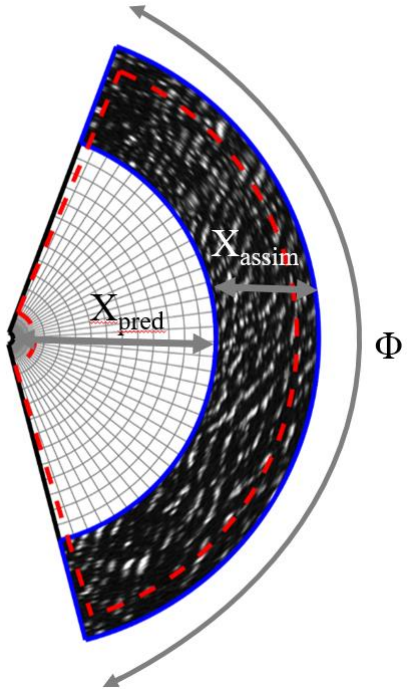

Figure 19. Diagram of Wavecast parameters.

The second forecast is available after the computation using the second observation period. This forecast will begin at the start of the second observation. The second forecast also begins with still water, because the waves from the first forecast have not yet arrived. Note that when the waves arrive, the forecasts contain overlapping waves. Configuring a domain such that forecasts contain overlapping waves is not necessary, although it would allow for though it will provide improved accuracy.

By the time the third forecast is available, waves have reached the origin, thus the entire forecast contains predicted waves. This will be the case for all proceeding forecasts. In this realistic schematic of Wavecast, each forecast can be predicted 75 seconds in advance. Thus, there is a continuous time series available of predicted waves 75 seconds before the actual waves arrive. This time horizon can be shortened or lengthened by manipulating the assimilation and domain size parameters depicted in this schematic. Additional influences on this time horizon will be the number of frequencies solved for in the MSEs (this schematic represents a solution using a single frequency), and the quality of the assimilated data. With lower quality assimilation data, for example with increased wave shadowing or noise, Δt_{comp} may increase slightly. However in the synthetic trials presented in this paper, with significant wave shadowing and noise, Δt_{comp} was only influenced on the order of several seconds.

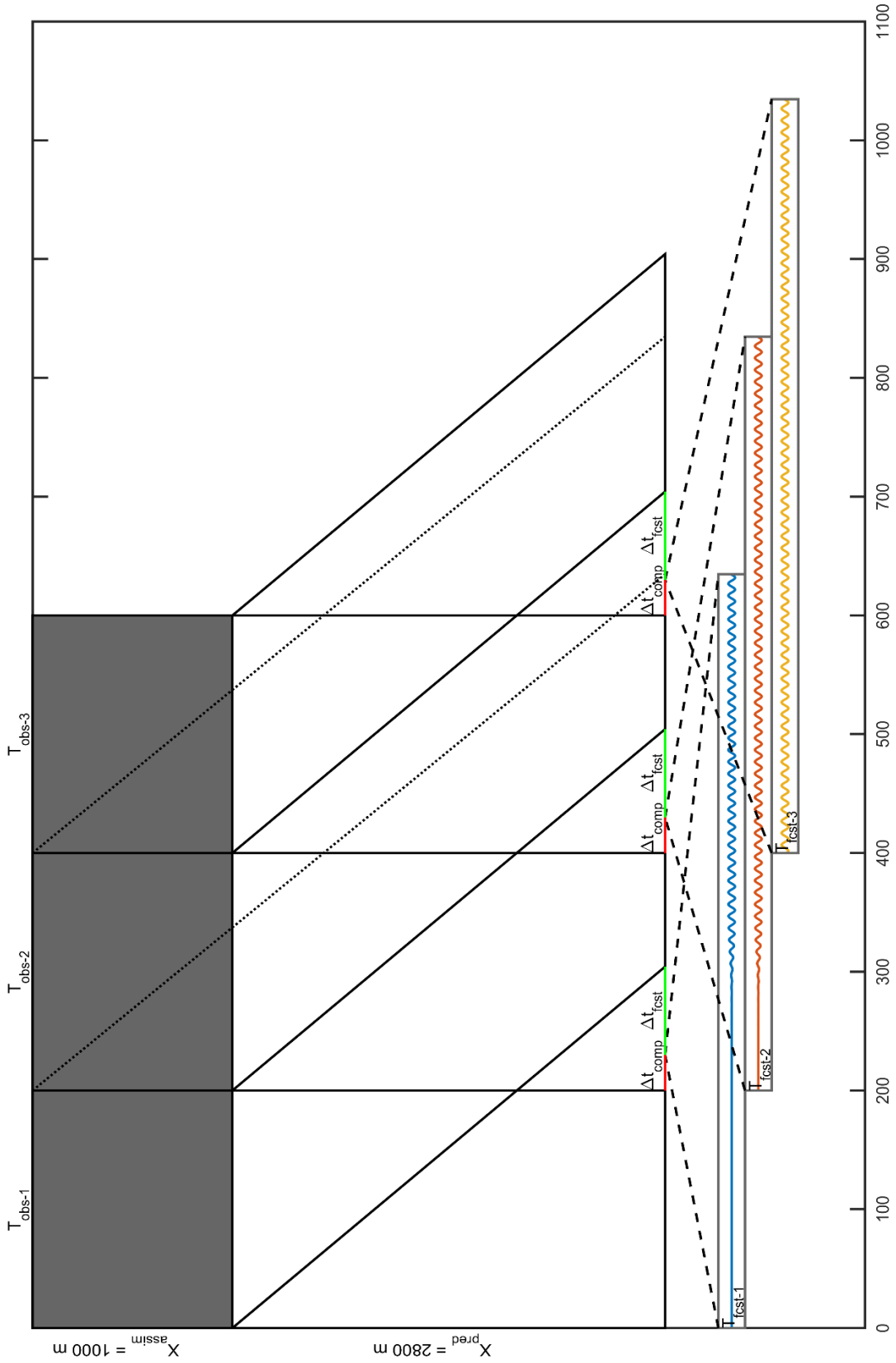

Figure 20. Schematic of constraints on model timing

4.7. Hardware Requirements and Cost Estimate

This work was originally benchmarked on the following system:

• 2 Quad-core Intel Xeon @ 2.67 GHz

• 94 GB DRAM

• Graphical Processing Unit Geforce GTX 680

- 1536 Cores @ 1058 MHz
- 4 GB DDR5 @ 192.2 GB/s Memory Bandwidth

During benchmarking the host computer utilized 1.5 CPU cores and 90 GB of RAM, the GPU utilized all 1536 GPU cores and 435 MB of RAM. This configuration achieved real-time forecasting over the domain and time scales shown in this report. Single-precision floating point computation is sufficient for this application, which means that commodity range GPU is acceptable. As indicated in Table 2, increasing the number of wave frequencies or the size of the assimilation and forecasting domains will increase computational requirements. A seven-fold increase in computational speed would be expected with the following hardware:

• GTX Titan X - top of the commodity/gamer range of GPUs ($1000)

• 3072 cores @ 1075 MHz, 12 GB DDR5 @ 336.5 GB/s Memory Bandwidth, Dual Slot

• Should provide 1.75x the performance of the benchmark system (memory BW limited).

• Host - 4 rackmountable towers can accommodate 4 dual-slot GPU, scale CPU to match GPU performance increase

• 4 GTX Titan X = 4 x 1.75 GTX680 7x increase over benchmark

• 1.5 CPU cores x 7 = 10.5 cores @ 2.7 GHz or greater

• 90 GB x 7 = 630 GB of memory

• Example system would be a Supermicro 7048GR-TR

- 2 Xeon CPUs with 16 cores @ 3.2 GHz
- 1 TB of DDR4 RAM
- 4 GTX Titan X cards

Estimated System Price: $30,000 (based on online information 2016)

Radar hardware: for this project we utilized a Si-Tex (*Radarpc25.9*) X-band imaging radar with a 9ft antenna. These systems are commercial off-the-shelf. We choose to use the largest available antenna in order to have the best azimuthal resolution and the highest power transmitter in order to have the largest radar range. In practice, a somewhat lower power transmitter and 6ft antenna could be used with likely limited detrimental impact.

Estimated Radar Price: $12,000 (quote from B&F Electronics, July 2016)

5. Accomplishments

The major accomplishment of this project is the development and verification of the Wavecast algorithm. In fulfillment of the objectives of the project, Wavecast provides a novel method of wave forecasting for application to Wave Energy Converter controls systems. The algorithm was verified against synthetic wave data and it was demonstrated that, if the wave model backbone contains the appropriate level of wave transformation processes, then accurate wave field reconstruction and forecasting is possible. This result is robust to the expected levels of wave shadowing and observational noise in the wave imaging marine radar observations. The algorithm represents a proof-of-concept for wave forecasting via radar data assimilation.

Additionally, development was accomplished in the areas of wave slope extraction from radar imagery, radar data assimilation, and GPU-based wave modeling and forecasting. These research accomplishments provide the necessary strides towards the realization of a commercial radar-based forecasting system.

Finally, a considerable amount of technical communication and dissemination to colleagues and industry was also conducted. Midway through the project we conducted a public webinar on the project that was attended by a number of industry participants and has led to follow-on work with industry this year. Publication citations and a complete list of presentations are listed below. Particularly notable, Alex Simpson received Best Oral Presentation awards at both the METS 2016 and YCSEC 2016 meetings.

5.1. Publications

- Simpson, A., M.C. Haller, D. Walker, P. Lynett, and R. Pittman. "Real-Time Wave-by-Wave Forecasting via Assimilation of Marine Radar Data", *Marine Energy Technology Symposium (METS 2016)*, extended abstract, 5 pages, 2016.
- Simpson, A. "Wave-by-Wave Forecasting via Assimilation of Marine Radar Data", *Master's Thesis*, School of Civil & Construction Engineering, Oregon State University, http://hdl.handle.net/1957/59904, 2016.
- Simpson, A., M.C. Haller, D. Walker, and P. Lynett, Wave-by-wave forecasting via assimilation of marine radar data, in preparation for *Journal of Oceanic and Atmospheric Technology*, 2017.

5.2. Presentations acknowledging DOE support

- Poster presentation: Simpson, A., Haller, M.C., Walker, D., Lynett, P., Pittman, R., and D. Honegger, "Assimilation of Wave Imaging Radar Observations for Real-Time Wave-by-Wave Forecasting", *Ocean Sciences Meeting*, February 21-26, 2016, New Orleans, LA, USA. Abstract ID: HI54A-1848.
- Oral Presentation: Simpson, A., "Real-Time Wave-by-Wave Forecasting via Assimilation of Marine Radar Data", *Marine Energy Technology Symposium*, April 25-27, 2016. Washington DC.

- Poster presentation: Simpson, A., "Wave-by-Wave Forecasting via Assimilation of Marine Radar Data", *Northwest National Marine Renewable Energy Center Annual Meeting*, September 19-20, 2016, Portland, OR, USA.
- Oral presentation: Haller, M., "Assimilation of Wave Imaging Radar Observations for Real-time Wave-by-Wave Forecasting", *Northwest National Marine Renewable Energy Center Annual Meeting*, September 17-18, 2015, Portland, OR, USA.
- Poster Presentation: Simpson, A., "Wave-by-Wave Forecasting via Assimilation of Marine Radar Data", *Northwest National Marine Renewable Energy Center Annual Meeting*, September 17-18, 2015, Portland, OR, USA.
- Poster Presentation: Simpson, A., "Wave-by-Wave Forecasting via Assimilation of Marine Radar Data", *International Network of Offshore Renewable Energy Symposium*, May 2015, Naples, Italy.
- Poster Presentation: Simpson, A., "Wave-by-Wave Forecasting via Assimilation of Marine Radar Data", *International Network of Offshore Renewable Energy Symposium*, October, 2015, Friday Harbor, WA, USA.
- Poster Presentation: Simpson, A., "Wave-by-Wave Forecasting via Assimilation of Marine Radar Data", *International Network of Offshore Renewable Energy Symposium*, October 2016, Orono, ME, USA.
- Oral Presentation: Simpson, A., "Wave-by-Wave Forecasting via Assimilation of Marine Radar Data", *Young Coastal Scientists and Engineers*, June 2016, Kingston, Ontario, Canada.

6. Conclusions

The major finding of this research is that a physics-based wave forecasting scheme, which relies on radar imagery as data for assimilation is a promising approach to wave-by-wave forecasting for WEC controls applications. An algorithm ("Wavecast") was developed and its performance was evaluated. Early in the project, performance tests definitively concluded that the system was capable of real-time forecasting, as the GPU-based wave model backbone is very computationally efficient. For verification of accuracy, a substantial set of synthetic wave data (i.e. forward runs of the wave model) were generated to be used as ground truth for comparison to the reconstructions and forecasts produced by Wavecast. For these synthetic cases, Wavecast demonstrated very good accuracy, for example, typical forecast correlation coefficients were between 0.84-0.95 when compared to the input data. Dependencies on shadowing, observational noise, and forecast horizon were also identified. While evaluation using synthetic datasets is only a preliminary conclusion, it has been shown that Wavecast is capable of real-time wave forecasting when the wave model physics accurately represent the observational environment and conditions.

During the second year of the project, a short field deployment was conducted in order to assess forecast accuracy under field conditions. The results of assimilating field data in Wavecast were less good due to technical challenges with the GPS heading accuracy, and considerable complexities in the environmental conditions on the day of data collection. An important lesson learned is that high-accuracy position and heading instrumentation should be used for radar image geo-rectification. This instrumentation is commercially available, but not standard on commercial

fishing vessels. Despite a lack in phase-resolved comparison, conclusions can be drawn from buoy-to-forecast spectral comparisons. During complex wave conditions (bimodal spectrum, perpendicular wind and wave directions), Wavecast is capable of qualitatively reconstructing both peaks in the spectrum. However, accurate reconstruction of the overall spectral wave energy has not yet been demonstrated and additional field tests are recommended.

Overall, wave-by-wave forecasting using data assimilation of radar imagery shows promise for short-term phase-resolved predictions. There are several challenges to be addressed before the system can be recommended for in-field use. The major barrier in this study was a lack of an adequate field dataset. This barrier was overcome for the purpose of this project through the creation of a substantial synthetic dataset. However, the immediate next-step on the path towards system commercialization is evaluation using a more robust field dataset. This evaluation will allow for improved understanding of forecast accuracy, as well as next-steps in optimization of computation timing. This project has served as a promising proof-of-concept for the approach to wave forecasting, and is a novel contribution to the optimization of Wave Energy Conversion devices.

7. Recommendations for Future Work

7.1. Inclusion of Nonlinear Correction terms in Wave Model

At present, the GPU-based wave model chosen for the forecasting algorithm is the linear Mild Slope Equations (MSEs). Nonlinear correction terms exist for the MSEs that enable extension of model applicability in more energetic sea states where nonlinearity is of increased importance. Nonlinear effects are also of increased importance in order to achieve longer forecast horizons, since they effect the wave speed, which has an integrated effect over longer forecast distances.

7.2. Additional Field Testing

The field study conducted through this project was done with limited resources, and was conducted during complex environmental conditions. The wind direction and wave direction were 90 degrees offset, and the sea state was starkly bimodal. Additionally, the GPS chosen for this study for its low-cost was not robust enough for adequate stabilization of the radar imagery. While the synthetic testing of Wavecast shows very promising performance in accuracy and model timing, further field testing of Wavecast is recommended. A radar dataset should be collected during a more simplistic sea state. Additionally, a more robust GPS should be used, such as those used for nautical applications that collect heading data from satellites as opposed to electronically. A device with at least 0.5 degree heading resolution and meter-scale positioning should be considered.

References

Belmont, M. R., Baker, J., & Horwood, J. M. K. (2003). Avoidance of phase shift errors in short term deterministic sea wave prediction. *Journal of Marine Engineering & Technology*, *2*(2), 21–26. http://doi.org/10.1080/20464177.2011.11020251

Belmont, M. R., Christmas, J., Dannenberg, J., Hilmer, T., Duncan, J., Duncan, J. M., & Ferrier, B. (2014). An examination of the feasibility of linear deterministic sea wave prediction in multidirectional seas using wave profiling radar: Theory, simulation, and sea trials. *Journal of Atmospheric and Oceanic Technology*, *31*(7), 1601–1614. http://doi.org/10.1175/JTECH-D-13-00170.1

Belmont, M. R., Horwood, J. M. K., Thurley, R. W. F., & Baker, J. (2006). Filters for linear sea-wave prediction. *Ocean Engineering*, *33*(17-18), 2332–2351. http://doi.org/10.1016/j.oceaneng.2005.11.011

Belmont, M. R., Horwood, J. M. K., Thurley, R. W. F., & Baker, J. (2008). Shallow angle wave profiling LIDAR. *Proceedings of the IEEE Working Conference on Current Measurement Technology*, 217–223. http://doi.org/10.1109/CCM.2008.4480871

Berkhoff, J. C. W. (1972). Computation of combined refraction-diffraction. In *Proc. 13th Coastal Eng. Conf.* (pp. 471–490). Vancouver.

Blondel, E., Ducrozet, G., Bonnefoy, F., & Ferrant, P. (2008). Deterministic reconstruction and prediction of non-linear wave systems. *23rd Int. Workshop on Water Waves and Floating Bodies*.

Fusco, F., & Ringwood, J. (2010a). A study on Short-Term Wave Forecasting for time-domain Control of Wave Energy Converters. *IEEE Transactions on Sustainable Energy*, *1*(2), 99–106.

Fusco, F., & Ringwood, J. V. (2010b). Short-term wave forecasting with ar models in real-time optimal control of wave energy converters. *IEEE International Symposium on Industrial Electronics*, 2475–2480. http://doi.org/10.1109/ISIE.2010.5637714

Halliday, J. R., Dorrell, D. G., & Wood, A. R. (2011). An application of the Fast Fourier Transform to the short-term prediction of sea wave behaviour. *Renewable Energy*, *36*(6), 1685–1692. http://doi.org/10.1016/j.renene.2010.11.035

Janssen, T. T., Van Dongeren, A. R., & Kuiper, C. (2001). Phase resolving analysis of multidirection wave trains. In *Ocean Wave Measurement and Analysis, Proc., 4th Int. Symp. Waves* (pp. 377–386). San Francisco, California. http://doi.org/10.1017/CBO9781107415324.004

Lyzenga, D. R., & Walker, D. T. (2015). A Simple Model for Marine Radar Images of the Ocean Surface. *IEEE Geoscience and Remote Sensing Letters*, *12*(12), 2389–2392.

Schoen, M. P., Hals, J., & Moan, T. (2011). Wave prediction and robust control of heaving wave energy devices for irregular waves. *IEEE Transactions on Energy Conversion*, *26*(2), 627–638. http://doi.org/10.1109/TEC.2010.2101075

Wu, G. (2004). Direct Simulation and Deterministic Prediction of Large-scale Nonlinear Ocean Wave-field, (1994), 258.

Zhang, J., Yang, J., Wen, J., Prislin, I., & Hong, K. (1999). Deterministic wave model for short-crested ocean waves: Part I. Theory and numerical scheme. *Applied Ocean Research*, *21*(4), 167–188. http://doi.org/10.1016/S0141-1187(99)00011-5

Appendix A: METS Extended Abstract. *Real Time Wave-by-Wave Forecasting via Assimilation of Marine Radar Data*

Executive Summary: A key task in Wave Energy Converter (WEC) development is to optimize device performance for commercial viability. For many of the proposed WEC designs, a promising optimization tool is an active controls system that tunes WEC functionality to the characteristics of the incoming wave field. This enables maximization of energy capture while protecting the system from extreme wave conditions. There has been considerable research in WEC control schemes, and a number of schemes depend on an accurate forecast for time horizons of several wave periods.

The work herein addresses the challenge of wave-by-wave forecasting for WEC control applications. Previous work of this type has been termed Deterministic Sea Wave Prediction (DSWP). DSWP methods are designed to predict water surface elevations highly resolved in time (wave-by-wave), as opposed to phase-averaged prediction of bulk wave properties (i.e. average wave height) over longer time scales. There are two main approaches to DSWP: prediction based on single-point measurements, such as from instrumentation mounted on the WEC, or prediction based on multi-point measurements at a distance and the subsequent reconstruction of the surrounding wave field. Our work herein falls under the latter category.

For this study, the multi-point wave measurements at a distance are derived from X-Band marine radar image time series. These observations typically span a circular footprint of several kilometers in radius, depending on wind and wave conditions. The radar collects image time series of backscatter intensity which are then converted to surface slope in the radar look direction (radial slope, η_r) using the method of Lyzenga and Walker. From radial slope time series throughout the domain, a best-fit wave model hindcast is determined and used as the initial conditions for the deterministic wave forecast. The wave model that we use for the hindcast and forecast is based on the Mild Slope Equation formulated in polar coordinates (Polar-MSE).

Appendix B: Master's Thesis. *Wave-by-Wave Forecasting via Assimilation of Marine Radar Data*

Executive Summary: A wave-by-wave forecasting system is desired for optimization of wave energy conversion devices and for improving safety of vessel-based marine operations. This study outlines the first validation attempts of a recently developed forecasting system called Wavecast. The forecasting approach uses X-Band marine radar images for data assimilation, then reconstructs and propagates the ocean wave field in both space and time using the Mild Slope Equation wave model. For data assimilation, the radial component of the sea surface slope is computed from the radar imagery using the recently-derived Radar Model (Lyzenga & Walker, 2015). The Radar Model is a direct relationship between radar backscatter intensity and radial slope, without the need for external calibration. Validation attempts of the forecasting system are carried out in two phases. First, synthetic data is used. Two trials are presented: a simple monochromatic dataset, and a nonlinear simulation of a realistic sea. Results of monochromatic testing show strong spectral correlation, and time series correlation of up to 0.9 throughout the full domain. Results of nonlinear testing show up to 83% spectral correlation of significant wave height, time series correlation up to 0.9 among reconstructed waves, but some decay in correlation among predicted waves. Next a field dataset is presented, which was collected by a ship-mounted radar offshore Newport, OR with spatial and temporal overlap to a TRIAXYS wave profiling buoy. The field dataset provides several challenges. Noise in the electronic compass readings prevented rectification of the ship's motion; however, this was overcome using a novel post-processing technique on the radar images to georeference each scan without the need for electronic compass readings. Additionally, uncertainty exists in the location of the TRIAXYS buoy; thus, a cross-correlation analysis was performed on a small region surrounding the buoy's anticipated location to determine the location of maximum correlation between actual and model time series. Despite complexities in the field dataset, assimilation of the field data in Wavecast shows good spectral reconstruction, with issues remaining in time series correlation. The presented validation attempts provide improved understanding of the accuracy and potential of Wavecast, and give support for the validity of the Radar Model.

Appendix C: Journal Submission. *Wave-by-Wave Forecasting via Assimilation of Marine Radar Data*

Executive Summary: This work describes a novel phase-resolving wave forecasting system. The developed system, referred to as Wavecast, couples an X-band marine radar with the linear Mild Slope Equations (MSEs) wave model for real-time reconstruction and forward propagation of the sea surface in space and time. Wave information is extracted from the radar image time series using a recently derived relationship between the radar backscatter intensity and the radial component of the sea surface slope (Lyzenga & Walker, 2015). The approach of Wavecast is to estimate a hindcast source function from the wave slopes in an annulus at the outer ranges of the radar imagery. The source function is subsequently propagated using the MSEs across a polar domain to a location of interest. When estimation and propagation of the source function are computed in faster than real time, a forecast is made at a location of interest within the polar domain. This paper covers theory, a description of Wavecast, phase-resolved synthetic validation, and spectral field validation using radar and in situ data collected offshore Newport, OR.